JCTC Journal of Chemical Theory and Computation

Development of a Polarizable Intermolecular Potential Function (PIPF) for Liquid Amides and Alkanes

Wangshen Xie,[†] Jingzhi Pu,[†] Alexander D. MacKerell, Jr.,*[,‡] and Jiali Gao*[,†]

Department of Chemistry and Supercomputing Institute, Digital Technology Center, University of Minnesota, Minneapolis, Minnesota 55455, and Department of Pharmaceutical Sciences, School of Pharmacy, University of Maryland, Baltimore, Maryland 21201

Received June 17, 2007

Abstract: A polarizable intermolecular potential function (PIPF) employing the Thole interacting dipole (TID) polarization model has been developed for liquid alkanes and amides. In connection with the internal bonding terms of the CHARMM22 force field, the present PIPF-CHARMM potential provides an adequate description of structural and thermodynamic properties for liquid alkanes and for liquid amides through molecular dynamics simulations. The computed heats of vaporization and liquid density are within 1.4% of experimental values. Polarization effects play a major role in liquid amides, which are reflected by an increase of 1.5−1.8 D in molecular dipole moment for primary and secondary amides. Furthermore, the computed polarization energies contribute to the total intermolecular interaction energy by 6−24%. The ability of the PIPF-CHARMM force field to treat protein backbone structures is tested by examining the potential energy surface of the amide bond rotation in *N*-methylacetamide and the Ramachandran surface for alanine dipeptide. The agreement with ab initio MP2 results and with the original CHARMM22 force field is encouraging, suggesting that the PIPF-CHARMM potential can be used as a starting point to construct a complete polarizable force field for proteins.

1. Introduction

Molecular mechanical force fields employing effective pairwise potential functions for electrostatic interactions are widely used and have been extremely successful in dynamics simulations of condensed-phase systems and biopolymers.[1,2] Undoubtedly, the most critical factor that determines the reliability of computational results is the accuracy of the potential energy functions. Consequently, there have been continuing efforts devoted to explicitly incorporate many-body polarization effects to further improve the accuracy of these force fields.[3−24] A straightforward approach for treating polarization effects in the current force fields is to include an induction term that depends on the instantaneous positions of the permanent charges and induction polarizations of the rest of the system.[25,26] Our goal is to incorporate explicit polarization terms into the CHARMM22 force field[27] by making adjustments to the nonbonded interaction terms and, at the same time, by minimizing the need for reparametrization of the internal bonding terms. We employ the same approach in the development of these force fields by first studying liquid properties of organic compounds representing different functional groups in proteins.[28] In this paper, we describe a polarizable intermolecular potential function (PIPF) for alkanes and amides.

One practical issue in developing a polarizable force field is that polarization effects are not uniquely described within the framework of classical force fields.[25,26] Thus, it is essential to first decide the functional form and the associated parameters to evaluate the polarization energy. Of course, molecular polarization is well-defined and can be

* Corresponding author e-mail: gao@chem.umn.edu.
[†] University of Minnesota.
[‡] University of Maryland.

10.1021/ct700146x CCC: $37.00
Published on Web 10/23/2007

properly treated by quantum mechanics (QM),[29,30] but its computational costs prevent it from applications to large molecular systems such as proteins and nucleic acids in aqueous solution.[31,32] Perhaps, the most widely used approach in molecular mechanics is based on the expression[25,26]

$$U_{\mathrm{pol}} = -\frac{1}{2}\sum_{i=1}^{N} \boldsymbol{\mu}_i \cdot \mathbf{E}_i^o \qquad (1)$$

where N is the number of interaction sites, $\mathbf{E}_i^o$ is the electric field at the ith atomic site due to the permanent charges of the system, and $\boldsymbol{\mu}_i$ is the induced dipole moment on the ith site. The associated parameters are the atomic polarizabilities which are given as a tensor. There is no rigorous way of defining these atomic polarizability tensors, and contributions due to higher order multipole moments are ignored or implicitly included by parametrization of eq 1. Despite these shortcomings, eq 1 provides a convenient approach to treat inductive polarization effectively as demonstrated by numerous studies in the past.[3−5,9−14,17,18,25,26,33−36] The present PIPF potential has been developed based on eq 1. In other studies, multipole moments have also been included in force field development.[18,19]

A closely related implementation is the Drude oscillator model (also called shell model),[20,37] which was originally introduced to treat dispersive interactions. In this approach, the partial charge on a polarizable site is redistributed among a set of off-center particles connected harmonically to the atomic site. The positions of these charge particles are determined self-consistently in response to the external field, and the charges and force constants are related to the atomic polarizability. Thus, the Drude oscillator model can be designed to yield the same results as the induced point dipole model.[20,37] Nevertheless, an additional choice must be made with respect to the number and distribution of these fictitious particles. The Drude model has been implemented into CHARMM, and efforts are being made to construct a complete force field for biopolymers.[20,21]

Both methods described above do not treat the charge-transfer effect, which has been suggested to be important for modeling proteins in aqueous solution.[38,] In recent years, the fluctuating charge model, which was derived on the basis of the principle of electronegativity equalization,[39−43] has been used by a number of groups to represent molecular polarization.[6,8,15,16,22−24,44] In this model, the values of the atomic charges are treated as dynamic variables, which can fluctuate subjected to the overall charge constraint and are dependent on the environmental electric field. In principle, the fluctuating charge model allows for charge transfer, although charge transfer between molecules in this model is often unphysical, and it is typically restricted within the same molecule to model charge polarization.[8,15,16,22] Kaminski et al. experimented with the combination of both fluctuating charges and point dipole induction.[15,16,44] It was concluded that the fluctuating charge model alone is inadequate in describing intermolecular interactions in a number of cases. The fluctuating charge model has also been implemented into CHARMM.[22−24]

A reasonable question that is often asked and was raised by an anonymous referee is whether or not there is a need for developing polarizable force field to study properties of systems that require a polarizable model. Indeed, most obvious thermodynamic quantities of simple liquids and solutions as well as biopolymers can be adequately described by effective potentials;[27,28] a convincing testimony is the widespread application and success of empirical force fields in biomolecular simulations. On one hand, it was thought that the seemingly anomalous behavior of alkylamine solvation was attributed to polarization effects,[33] but it was later shown that a reparametrization of the effective pairwise potential can indeed reproduce experimental results.[33e] On the other hand, the solvation of a chloride ion by a water sphere is dependent on the use of a pairwise potential or a polarizable model, and only the latter can produce results consistent with expectation.[34] Although little experimental information is available, undoubtedly, the simulation of protein folding will benefit from the use of a polarizable force field, because the charge distribution due to polarization for a fully solvent exposed peptide will be different than that when it is folded in the interior of the protein. Pairwise, effective potentials cannot capture these internal charge polarizations, whereas a carefully developed polarizable force field is more likely to be successful. The answers to these questions will continue to emerge as more tests and simulations are carried out using polarizable force fields.

In the following, we describe the results from molecular dynamics simulations of liquid alkanes and amides, making use of the PIPF potential for nonbonded interactions and the CHARMM22 force field for the remainder of the energy terms. We designate this combined force field as PIPF-CHARMM. Amides represent an important class of organic compounds as model systems for peptides, and it is essential to reproduce structural and energetic properties of these liquids in order to construct a force field for polypeptides. This is reflected in the development of a number of force fields, including the effective CHARMM[27] and OPLS force fields,[28,45] and the fluctuating charge model within CHARMM.[22] Although both alkanes and amides potentials have been developed, we focus our discussion on liquid amides, including formamide (primary amide), *N*-methylacetamide (NMA), and *N*-methylformamide (NMF, secondary amides), and *N*,*N*-dimethylformamide (DMF, tertiary amide). We first describe the polarization model that we use, followed by parametrization and computational details. In section 4, we present Results and Discussion. In section 5, we summarize the major findings of this work.

2. Theoretical Model

We employ the "standard" CHARMM force field plus a polarization term as follows[1,27]

$$U(\mathbf{R}) = \frac{1}{2}\sum_{\text{bonds}} K_b(b-b_0)^2 + \frac{1}{2}\sum_{\text{angles}} K_\theta(\theta-\theta_0)^2 + \frac{1}{2}\sum_{\text{UB}} K_{\text{UB}}(S-S_0)^2 + \frac{1}{2}\sum_{\text{dihedrals}} K_\varphi(1-\cos(n\varphi-\delta)) + \frac{1}{2}\sum_{\text{impropers}} K_\omega(\omega-\omega_0)^2 + \sum_{\text{nonbonded pairs}} \left\{\epsilon_{ij}^{\min}\left[\left(\frac{R_{ij}^{\min}}{r_{ij}}\right)^{12} - 2\left(\frac{R_{ij}^{\min}}{r_{ij}}\right)^{6}\right] + \frac{q_i q_j}{4\pi\epsilon_0\epsilon r_{ij}}\right\} - \frac{1}{2}\sum_{\text{atoms}} \boldsymbol{\mu}_i\cdot\mathbf{E}_i^o \quad (2)$$

where the potential energy, $U(\mathbf{R})$, is a sum over the internal and nonbonded terms as a function of the atomic coordinates $\mathbf{R}$. The internal terms include bond (b), valence angle (θ), Urey−Bradley (UB, S), dihedral angle (φ), and improper angle (ω) contributions, as shown in eq 2. The parameters K_b, K_θ, K_{UB}, K_φ, and K_ω are the respective force constants, and the variables with the subscript "0" are the corresponding equilibrium values. The nonbonded terms include Coulomb, induction (eq 1), and van der Waals interactions in the form of the Lennard-Jones potential. The variables in eq 2 have standard meanings,[1,27] and they are not explicitly described here in view of brevity.

We adopt the Thole interaction dipole (TID) model[46] in the present PIPF potential, which yields excellent results in the predicted molecular polarizabilities with a set of purely atomic isotropic polarizability parameters. Furthermore, it has been shown that these parameters are remarkably transferable and can provide a reasonable estimate of the anisotropy in molecular polarizability even though atomic isotropic parameters are used.[46,47] In the TID model, the induced dipole at the ith interaction site due to the homogeneous external electric field $\mathbf{E}_i^o$ is given by

$$\boldsymbol{\mu}_i = \alpha_i(\mathbf{E}_i^o - \sum_{j\neq i}^{N} \mathbf{T}_{ij}\cdot\boldsymbol{\mu}_j) \quad (3)$$

where N is the number of polarizable sites, α_i is the atomic polarizability tensor, and $\mathbf{T}_{ij}$ is the dipole field tensor defined by

$$\mathbf{T}_{ij} = \frac{1}{r_{ij}^3}\mathbf{I} - \frac{3}{r_{ij}^5}\begin{bmatrix} x^2 & xy & xz \\ yx & y^2 & yz \\ zx & zy & z^2 \end{bmatrix} \quad (4)$$

where $\mathbf{I}$ is the identity matrix, and x, y, and z are the Cartesian components along the vector between atoms i and j at a distance r_{ij}. In principle, all atomic interactions can be included within the same molecule, although short-range interactions (1−2, 1−3 and 1−4 terms) are excluded in the present study.

To avoid infinite polarization at a distance shorter than $(4\alpha_i\alpha_j)^{1/6}$ between two interacting induced dipoles, a phenomenon called the "polarization catastrophe", Thole[46] introduced a damping scheme in which the dipole field tensors can be derived from the first-order elements

$$(\mathbf{T}_{ij})_p^D = -(1-e^{-au^3})\frac{(\mathbf{r}_{ij})_p}{r_{ij}^3} \quad (5)$$

where the subscript p is a Cartesian component of the vector $\mathbf{r}_{ij}$, and the superscript D denotes a damped interaction tensor. The damping scheme is equivalent to considering a smeared charge distribution between two interacting sites whose charge distribution is given as follows[46,47]

$$\rho(u_{ij}) = \frac{3a}{4\pi}e^{-au_{ij}^3} \quad (6)$$

where $u_{ij} = r_{ij}/(\alpha_i\alpha_j)^{1/6}$ is the effective distance between sites i and j. The factor a is a dimensionless width parameter of the smeared charge distribution which controls the strength of damping. The damping factor used in the PIPF is a = 0.572.

The modified higher-order $\mathbf{T}$ matrix elements can be obtained successively by taking the derivative of the preceding lower rank elements

$$(\mathbf{T}_{ij})_{pq}^D = \nabla_p(\mathbf{T}_{ij})_q^D = \lambda_5\frac{3(\mathbf{r}_{ij})_p(\mathbf{r}_{ij})_q}{r_{ij}^5} - \lambda_3\frac{\delta_{pq}}{r_{ij}^3} \quad (7)$$

$$(\mathbf{T}_{ij})_{pqr}^D = \nabla_p(\mathbf{T}_{ij})_{qr}^D = -\lambda_7\frac{15(\mathbf{r}_{ij})_p(\mathbf{r}_{ij})_q(\mathbf{r}_{ij})_r}{r_{ij}^7} + \lambda_5\frac{3[(\mathbf{r}_{ij})_p\delta_{qr} + (\mathbf{r}_{ij})_q\delta_{pr} + (\mathbf{r}_{ij})_r\delta_{pq}]}{r_{ij}^5} \quad (8)$$

where the parameters λ_i are given as follows

$$\lambda_3 = 1 - \exp(-au^3) \quad (9)$$

$$\lambda_5 = 1 - (1+au^3)\exp(-au^3) \quad (10)$$

$$\lambda_7 = 1 - \left(1 + au^3 + \frac{3}{5}a^2u^6\right)\exp(-au^3) \quad (11)$$

As in the procedure used by Ren and Ponder[17,18] interactions are damped only between interacting induced dipoles, while the electric field due to the permanent charges is not affected.

Equation 3 shows that each induced dipole depends on the polarization of all other dipoles. Thus, it must be solved self-consistently. A standard iterative procedure is often used such that an initial guess of the induced dipoles (or simply set to 0) is first made to estimate a set of induced dipoles, which are inserted into eq 3 to yield a newer set of induced dipoles. These induced dipoles are then used in the next iteration, and the process continues until a predefined convergence criterion is satisfied.[10−14] Typically, a few iteration steps are sufficient to achieve the required accuracy to ensure energy conservation, and the iterative procedure provides the most practical, converged results in molecular dynamics simulations.[10−14] Alternatively, eq 3 can be rearranged such that the induced dipole moments are determined exactly by inverting the dipole interaction matrix[10]

$$\boldsymbol{\mu} = \mathbf{A}^{-1}\mathbf{E}^o \quad (12)$$

where $\boldsymbol{\mu}$ is the column induced dipole vector, $\mathbf{E}^o$ is the electric field matrix due to atomic partial charges, and the interaction matrix $\mathbf{A}$ is defined as

$$\mathbf{A} = \begin{bmatrix} \alpha_1^{-1} & \mathbf{T}_{12} & \cdots & \mathbf{T}_{1N} \\ \mathbf{T}_{21} & \alpha_2^{-1} & \cdots & \mathbf{T}_{2N} \\ \vdots & \vdots & \ddots & \vdots \\ \mathbf{T}_{N1} & \mathbf{T}_{N2} & \cdots & \alpha_N^{-1} \end{bmatrix} \tag{13}$$

Although eq 12 yields the exact results, which is useful for validating the results from the iterative procedure, the shortcoming is the unbearable computation costs for large systems, which scales as $27 \times N^3$ to invert the $\mathbf{A}$ matrix ($3N \times 3N$-dimension).[9]

If one treats the induced dipoles as independent dynamic variables, the nuclear dynamics and molecular polarization can be propagated simultaneously. Sprik and Klein,[37] among others, have used this approach to perform molecular dynamics simulations with an induced polarizable dipole force field. In this case, the Lagrangian of the system is extended with a fictitious kinetic term associated with these extra variables, and the dynamics of the induced dipole moment is governed by the following equation of motion (in matrix form)[48]

$$\mathbf{m}_\mu \ddot{\boldsymbol{\mu}} = \mathbf{E} - \frac{\boldsymbol{\mu}}{\alpha} \tag{14}$$

where $\mathbf{m}_\mu$ is an "inertial factor" associated with the extra dynamical variables whose dimensions are those of mass $\times$ charge^{-2}, $\mathbf{E}$ is the total electric field, and $\ddot{\boldsymbol{\mu}}$ is the second time derivative of the induced dipole. In comparison with solving the self-consistent equations, this approach is a very efficient way of computing induced dipoles with an increase in computer time by a factor of about 2.[48] As pointed out by Van Belle et al.,[48] the induced dipoles will fluctuate about its average orientation during the dynamics simulations, although the converged induced dipoles are always oriented along the direction of the local electric field.

All three methods have been implemented into the program CHARMM (c33a1) for the TID model, and a critical evaluation of their performance and convergence in computed thermodynamic and structural properties has been carried out (to be published).

3. Computational Details

3.1. Parametrization. The parametrization of the PIPF-CHARMM force field follows the procedure employed previously in the development of the original CHARMM22 force field.[27] For convenience, the internal terms and nonbonded terms are optimized iteratively. Experimental structural data and bulk liquid properties for different organic functionalities are used as the primary targets of parameter optimization. Potential energy surfaces, relative energies of different conformations, and vibrational spectra calculated from high level QM methods are used as Supporting Information where experimental results are not available.

3.1.1. Nonbonded Terms. Nonbonded terms include van der Waals interactions, which are modeled by the Lennard-Jones form in CHARMM, Coulomb interactions among fixed (permanent) atomic partial charges, and polarization interactions, which include both charge-induced dipole and induced dipole−induced dipole contributions. We used the Lennard-Jones parameters from the CHARMM22 force field as an initial input for the same types of interaction site,[27] whereas the partial atomic charges are scaled to yield the correct dipole moments in the gas phase, using the TID model, for the model compounds selected in the present study. The original set of isotropic atomic polarizabilities was fitted for H, C, N, and O to a set of 16 molecular polarizabilities,[46] and later, van Duijnen and Swart extended the optimization set to 52 molecules with halogen and sulfur atoms.[47] Although different optimization schemes were used, they found that the original set was very similar to those from the new optimization.[47] We have also tried to reoptimize these atomic polarizabilities and reached the same conclusion. Thus, we decided to directly use the atomic polarizabilities from Thole's work.[46]

Then, condensed-phase simulations were carried out by slightly readjusting the Lennard-Jones parameters and partial charges to reproduce the experimental heats of vaporization and liquid densities. Consequently, the finals set of charges and atomic polarizabilities do not yield the exact, although very close, gas-phase dipole moments for these amides. The optimized parameters are given in Table S1, Supporting Information.

3.1.2. Internal Terms. Having optimized an initial set of the nonbonded parameters for alkanes and amides, we further examined the internal energy terms, including bond stretching, angle bending, out-of-plane bending, and torsion of dihedral angles, using the original values in the CHARMM22 force field.[27] We focused on the torsional potential energy surface and vibrational frequencies of NMA and the conformational energies and the Ramachandran map of alanine dipeptide obtained from QM calculations at the LMP2/cc-pVQZ(-g)//MP2/6-31G(d) level of theory.[49] Then, we returned to liquid simulations to further optimize the nonbonded energy terms until both liquid-phase results and internal energy terms are satisfactory. Finally, to match the ab initio Ramachandran map, an energy correction map (CMAP)[49] is also made to the φ, ψ dihedrals using the PIPF-CHARMM force field. For additional details of the CMAP procedure, readers are directed to the original paper.[49] The final force field is given as Supporting Information, which can be download as the parameter file for CHARMM.

3.2. Simulation Details. Nonbonded parameters were optimized through liquid simulations of four alkanes and six amides. In each case, molecular dynamics were executed with the CHARMM program using the isothermal−isobaric (NPT) ensemble at 1 atm and a temperature indicated below. The temperature is maintained by the Nose-Hoover thermostat,[50] while the pressure is controlled via the Langevin piston method.[51] The velocity Verlet algorithm was used to integrate the equations of motion with a time step of 1 fs.[52] In the present PIPF potential employing the TID model for molecular polarizations, intramolecular interactions between atom pairs that form a covalent bond (1−2), a bond angle (1−3), and a dihehdral angle (1−4) are excluded from the

Table 1. Optimized Parameters for Alkanes and Amides in the Nonbonded Energy Terms of the Present PIPF Potential along with the Original Values in the CHARMM Force Field

	$R_{min}/2$ (Å)		ϵ (kcal/mol)		q (e)		α (Å^3)
atom type	CHARMM	PIPF	CHARMM	PIPF	CHARMM	PIPF	PIPF
C(R−CH3)	2.040	2.020	−0.078	−0.080	−0.27	−0.09	1.334
C(R2−CH2)	2.175	2.120	−0.055	−0.060	−0.18	−0.06	1.334
C(R3−CH)	2.275	2.200	−0.027	−0.035	−0.09	−0.03	1.334
C(O═C−CH3)	2.060	2.020	−0.080	−0.080	−0.27	−0.09	1.334
C(N2°−CH3)	2.060	2.020	−0.080	−0.080	−0.11	0.02	1.334
C(N3°−CH3)	2.060	2.020	−0.080	−0.080		0.05	1.334
C(O═C)	2.000	1.960	−0.110	−0.110	0.51	0.45	1.334
O(C═O)	1.700	1.730	−0.120	−0.120	−0.51	−0.45	0.837
N(N1°)	1.850	1.850	−0.200	−0.200	−0.64	−0.68	1.073
N(N2°)	1.850	1.850	−0.200	−0.200	−0.47	−0.49	1.073
N(N3°)	1.850	1.850	−0.200	−0.200		−0.46	1.073
H(N1°)	0.2245	0.7577	−0.046	−0.015	0.32	0.34	0.496
H(N2°)	0.2245	0.7577	−0.046	−0.015	0.31	0.29	0.496
H(C═O)	1.320	1.340	−0.022	−0.025	0.08	0.00	0.496
H(R−CH3)	1.320	1.340	−0.022	−0.025	0.09	0.03	0.496
H(N−CH3)	1.320	1.340	−0.022	−0.025	0.09	0.06	0.496
H(O═CCH3)	1.320	1.340	−0.022	−0.025	0.09	0.03	0.496

dipole interaction tensor. We have also examined the possibility to include 1−4 interactions in molecular polarization, but we found that the best results are obtained without these short-range terms. We employed the iterative procedure to converge the induced dipoles with a criterion of less than 0.0001 Debye per atom. In all simulations, a spherical cutoff was used to generate a nonbonded list for all pairs within 12.5 Å, and the interaction forces are smoothed to 0 by a switching function between 11.0 and 12.0 Å for Coulomb interactons and a shifted potential for Lennard-Jones interactions.[53c] Although the use of a spherical cutoff for nonbonded interactions may introduce some errors in the computed thermodynamic properties, the development of the OPLS and the CHARMM22 force fields as well as the SPC, the TIP3P, and the TIP4P models utilized even shorter truncation distances at that time. Yet, numerous applications suggest that these force fields still perform exceptionally well when long-range electrostatics is explicitly included. Certainly, models that are specially derived for Ewald calculations have shown improved properties, especially in computed dielectric constants.[53] We are currently implementing the PME-based method for the present model to further validate the present parameters. Spherical truncation was made at 12.5 Å for interactions involving induced dipoles. All the bonds connecting to a hydrogen atom are fixed by the SHAKE algorithm.[54]

In each case, a cubic box was used, consisting of 256 molecules with periodic boundary conditions. The box size varied from about 26 × 26 × 26 Å^3 for formamide to as large as 35 × 35 × 35 Å^3 for isobutane. The simulations were run for ethane, propane, and butane at their boiling points, which are 184, 231, and 273 K, respectively; for isobutane, formamide (FORM), and *N*-methylformamide (NMF) at 298 K; for acetamide (ACEM) at 373 K and its boiling point (494 K); for *N*-methylacetamide (NMA) and *N*,*N*-dimethylacetamide (DMA) at 373 K; and for *N*,*N*-dimethylformamide (DMF) at 298 and 373 K. Each system was first equilibrated by at least 1 ns, followed by another 1 ns for averaging. Tests suggest that the computed results are sufficiently converged and show little variations at much longer simulation time for these simple liquid systems. Statistical uncertainties ($\pm 1\sigma$) for the computed properties reported here are determined through averages of batches of 50 ps simulations.

The average energy of the gas-phase molecule was calculated by Monte Carlo (MC) simulations of a single molecule at the same temperature as in the corresponding MD simulations. Standard Metropolis sampling[2] was used that included Cartesian moves for all atoms. Each Monte Carlo simulation consisted of at least 1×10^6 configurations of equilibration followed by 5×10^6 configurations of averaging. The energy convergence for a single molecule in the gas phase is much better achieved employing Monte Carlo simulations than using molecular dynamics where large fluctuations in temperature complicate potential energy convergence.

4. Results and Discussion

4.1. Polarization. Optimized nonbonded parameters are listed in Table 1. In general, partial charges are smaller than those in the CHARMM22 force field. This is expected since the fixed charge force field mimics many-body polarization effects in an average way such that the molecular dipoles are greater than those in the gas phase. Except for the hydrogen atom on nitrogen, the Lennard-Jones parameters in the present PIPF potential are very similar to the original values in CHARMM.[27] The "polar" hydrogen radius was increased from 0.2245 to 0.7577 Å (for type H only in the CHARMM force field definition in the present set of compounds). Atomic polarizabilities for each element are directly taken from the TID model,[46] which were fitted to experimental *anisotropic* molecular polarizabilities for a small set of molecules in the gas phase,[47] but they require

Table 2. Computed and Experimental Dipole Moment and Molecular Polarizability for Amides[a]

	μ_g (gas phase)		μ_{tot} (liquid)		μ_{ind} (liquid)		α (Å^3)	
liquid	exp[b]	PIPF	PIPF	QM/MM[d]	PIPF	QM/MM[d]	exp[b]	PIPF
formamide	3.73	3.70	5.3	4.9	1.6	1.2	4.08	4.08
acetamide	3.68	3.59	5.4, 5.1[c]		1.8, 1.5		5.67	5.91
NMA	3.72	3.31	5.0	4.7	1.7	0.9	7.82	7.97
NMF	3.83	3.35	4.9	4.4	1.5	1.2	5.91	5.91
DMA	3.70	3.31	4.4		1.1		9.63	9.24
DMF	3.82	3.48	4.4, 4.3[c]	4.6	0.9 ,0.8	0.5	7.81	7.81

[a] Dipole moment in Debye, polarizability in Å^3. [b] Experimental data are from ref 42. [c] Corresponding to simulations at the second (higher) temperature (see text). [d] Computed using the AM1 model for each amide in its liquid treated by the polarizable model in ref 14.

Table 3. Computed Energetic Results (kcal/mol) for Alkanes and Amides at Specified Temperatures[a]

species	$-\Delta E_i$	$-\Delta E_{elec}$	$-\Delta E_{pol}$	ΔE_{intra}	$-\Delta E_{tot}$	ΔH_v(exp)[b]	ΔH_v(calc)
ethane (184)	3.12	0.00	0.01	−0.03	3.10	3.52	3.46 ± 0.02
propane (231)	4.03	−0.01	0.01	−0.04	3.99	4.49	4.45 ± 0.04
butane (273)	4.90	0.02	0.01	−0.05	4.85	5.35	5.39 ± 0.05
isobutane (298)	4.09	0.01	0.01	−0.02	4.06	4.57	4.66 ± 0.06
FORM (298)	14.41	7.84	3.51	−0.01	14.40	14.7	14.99 ± 0.03
ACEM (373)	14.35	6.58	3.41	0.06	14.41		15.16 ± 0.04
ACEM (494)	12.10	5.38	2.84	0.12	12.22	13.4	13.20 ± 0.05
NMA (373)	12.83	4.46	2.11	−0.09	12.73	13.3[c]	13.48 ± 0.05
NMF (298)	12.93	5.21	2.37	0.00	12.93	13.52	13.55 ± 0.04
DMA (298)	12.24	2.73	0.77	0.21	12.46	12.7	13.05 ± 0.03
DMF (298)	10.95	2.89	0.65	0.10	11.05	12.00	11.79 ± 0.03
DMF (373)	9.72	2.54	0.61	−0.04	9.68	10.4	10.42 ± 0.04

[a] Temperatues are indicated in parentheses in Kelvin. [b] Experimental data are from refs 42 and 49. See text for discussion. [c] Reference 62. Experimental heat of vaporization for *N*-methylacetamide has been reported at 14.2 kcal/mol (ref 57).

no further modification in liquid simulations. Importantly, only a single parameter (isotropic atomic polarizability) is needed for each element for all interaction types. The remarkable transferability of the TID model has been thoroughly examined by van Duijnen and Swart.[47] The transferability is a major advantage of the TID model, for which few other polarizable models exhibit such a good behavior.

Table 2 depicts the computed molecular dipole moments in the gas phase and in the liquid phase along with the average molecular polarizabilities for amides, for which all intramolecular interactions are included in the calculation. The computed molecular polarizabilities are in excellent agreement with experimental results. Gas-phase dipole moments are generally underestimated in the present TID model, with a mean unsigned error of less than 8% in comparison with the experimental data.[55−57] This is in contrast to the effective pairwise potentials, in which the molecular dipoles are typically overestimated by 10−20% to account for polarization effects.[1,27,28] In the present study, we decided not to strictly enforce the requirement that gas-phase dipole moments exactly reproduce the corresponding experimental data. Our experience from early studies[13,14] shows that the increased flexibility allows for condensed-phase properties to be better described, and similar observations have been made in recent applications.[22] Clearly, the dipole moments are greatly enhanced in going into the liquid phase, although the quantitative accuracy of the average dipole moments in the fluid phase is difficult to assess because there are no experimental data for comparison. As expected, the enhancement in dipole moment for the primary and secondary amides is more significant than that for the tertiary amides due to hydrogen bonding interactions in the former, which are absent in the latter systems. Previously, a similar trend was observed from Monte Carlo simulations of formamide, acetamide, *N*-methylformamide, and *N*-methylacetamide using a polarizable intermolecular potential function (PIPF-A)[14] with a set of atomic polarizabilities similar to the Applequist[58] values without considering intramolecular polarization interactions. However, the present TID model (Table 2) yields induced dipoles twice as large as the previous PIPF-A potential.[14] The present results are in better agreement with combined QM/MM simulations in which one solute is represented by the semiempirical AM1 method embedded in a solution of the same amide.[14] For the primary and secondary amides the computed induced dipoles are 0.9−1.2 D from the QM/MM simulations.[14]

4.2. Liquid Properties. The computed energetic results are summarized in Table 3. The heat of vaporization is related to the total intermolecular interaction energy of the liquid, E_i(l), the intramolecular energies in the liquid, E_{intra}(l), and in the gas phase, E_{intra}(g), and the work term, which is RT for 1 mol of ideal gas.

$$\Delta H_v(T) = -E_i(\mathrm{l}) - E_{intra}(\mathrm{l}) + E_{intra}(\mathrm{g}) + RT$$
$$= -E_{tot}(\mathrm{l}) + E_{intra}(\mathrm{g}) + RT \qquad (15)$$

In computing the intermolecular interaction energy for the liquid, we have included a correction for long-range van der Waals interactions beyond the cutoff distance by assuming the distribution function is uniform.[14,59] The correction to

Table 4. Computed and Experimental Molecular Volume, Diffusion Constants, and Dielectric Constant for Simulated Liquids[a]

	V (Å^3)		D (10^{-9} m^2/s)		ϵ	
species	exp	calc	exp	calc	exp	calc[b]
ethane (184)	91.5	91.3 ± 0.4	4.27 (182)	4.66 ± 0.02		
propane (231)	126.0	127.4 ± 1.2	5.13 (243)	4.86 ± 0.05		
butane (273)	160.3	162.1 ± 1.6		5.00 ± 0.02		
isobutane (298)	175.1	178.1 ± 2.6		6.89 ± 0.09		
FORM (298)	66.3	65.0 ± 0.2		0.41 ± 0.01	109.5	138
ACET (373)	99.9	96.8 ± 0.3		0.75 ± 0.004		154
ACET (494)		108.0 ± 0.5		2.90 ± 0.03		145
NMA (373)	135.8	132.4 ± 0.6	1.47 (373)	1.46 ± 0.02	101	152
NMF (298)	98.3	97.8 ± 0.3	0.85 (298)	0.72 ± 0.01	186	200
DMA (298)	154.5	153.1 ± 0.3	1.37 (298)	0.57 ± 0.004	38.9	116
DMF (298)	128.5	128.9 ± 0.4	1.64 (298)	1.08 ± 0.01		
DMF (373)	139.0	139.7 ± 0.7	3.93 (373)	2.67 ± 0.02		165

[a] Temperatues are indicated in parentheses in Kelvin. Experimental data are from refs 42, 49, and 50. [b] Since the simulation is relatively short for computing the slowly converging total molecular dipole moment, it is likely that the computed dielectric constants have not fully converged. Further simulations are being carried out.

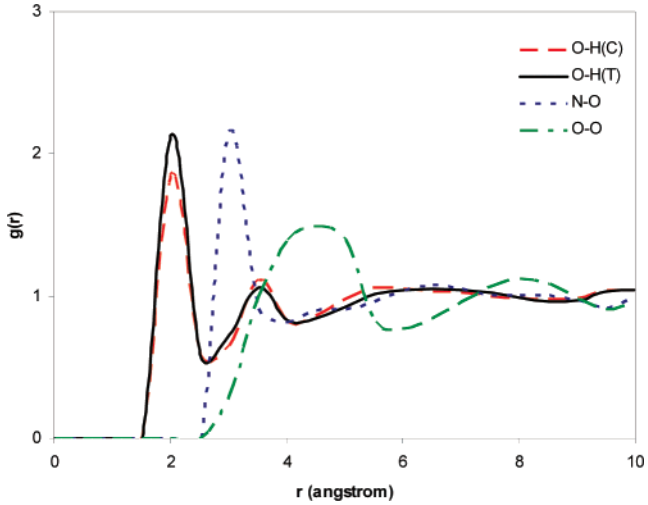

Figure 1. Computed O−H(C), O−H(T), N−O, and O−O radial distribution functions for liquid formamide at 25 °C. H(C) and H(T) specify the amino hydrogen atoms cis and trans to the carbonyl group. Distances are in angstroms.

the computed heat of vaporization due to departure from ideal behavior of the vapor was found to be negligible for amides, and thus they are not included.[60,61] The mean unsigned error in the calculated heats of vaporization for the four alkanes and six amides (two performed at two termperatures) is 1.4% compared to the experimental data.[55−57,62−66] For comparison, the average error reported by Jorgensen et al. is about 2% for hydrocarbons and amides for the OPLS-AA potentials.[28] Simulation of liquid alkanes and amides using CHARMM fixed charge force field yields an error ranging from 0 to 6%.[22] In a separate study employing the PIPF-A potential,[14] the average error was about 2% for four amides, formamide, NMF, NMA, and DMF.[14] Thus, the present energetic results are comparable to or slightly better than the performance of earlier force fields. It should be noted that we have used 100% of the trans configuration for NMA and NMF, and they remained in that configuration, whereas there are about 2−3% of the cis population in natural abundance in experiments.[67,68]

Table 3 also lists the average polarization energies in these liquids. Obviously, there is little contribution from molecular polarization in liquid alkanes, whereas polarization effects are significant in liquid amides. The largest polarization contributions are found in primary and secondary amides, amounting to about 24% and 18% of total intermolecular interaction energy, respectively. For comparison, the PIPF-A model has polarization effects between 12 and 14% of the total energy for primary and secondary amides.[14] In that model, the gas-phase dipole moments for these amides are slightly greater than the corresponding experimental value except NMF,[14] whereas they are smaller in the present case.

Table 4 lists the computed liquid density (volume), self-diffusion constants, and dielectric constants at various temperatures used in the dynamics simulations. The mean unsigned error in the computed molecular volume and liquid density is about 1.3% in comparison with experimental data (Table 4). Overall, the TID model shows excellent results for these organic liquids. We note that during the parametrization process, DMF was only considered at 373 K. Interestingly, when these parameters are used to perform simulations of DMF at 298 K, we obtain a liquid density and ΔH_v within 1% and 2% from the corresponding experimental values. The dielectric constants have only been averaged for 1 ns of simulation time, and they are almost certain not yet converged. Extended simulations with particle-mesh Ewald treatment of long-range electrostatics are being carried out. The calculated self-diffusion coefficients are somewhat underestimated for NMF, DMF, and DMA, while it is in excellent agreement with experiment for NMA.[69,70] For comparison, the CHARMM-FQ model yields a value of $D = 1.93 \times 10^{-9}$ m^2/s for liquid NMA. The effective CHARMM force field produced a value of 2.04×10^{-9} m^2/s.[27]

4.3. Radial Distribution Functions. The structure of the liquids are characterized by radial distribution functions (rdfs), $g_{xy}(r)$, which specifies the probability of finding an atom y at a distance r from atom x. All rdfs are normalized to the bulk density. To simplify our discussion, we focus on rdfs involving hydrogen bonding interactions. Errors associated with data collection are about half of the width of the bin size, which is 0.05 Å.

4.3.1. Formamide and Acetamide. Figure 1 shows the radial distribution functions for liquid formamide, in which the hydrogen atom trans to the carbonyl group is denoted by H(T) and cis to the carbonyl group by H(C). The strong first peaks of the carbonyl oxygen and amide hydrogen pairs, O−H(C) and O−H(T), centered at 1.95 Å are due to hydrogen bonding interactions. The results are in excellent agreement with the peak at 1.9 Å assigned to O−H contacts from diffraction experiments.[71−74] In an early study using the PIPF potential, the first O−H peak in liquid formamide occurs at 1.85 Å.[14] The agreement with the OPLS[28] and CHARMM[27] potentials is also good with the first peak occurring at 1.9 Å. Integration to the minima of the first peaks gives 0.9 and 1.0 nearest neighbors around H(C) and H(T). For comparison, other studies using PIPF potential give

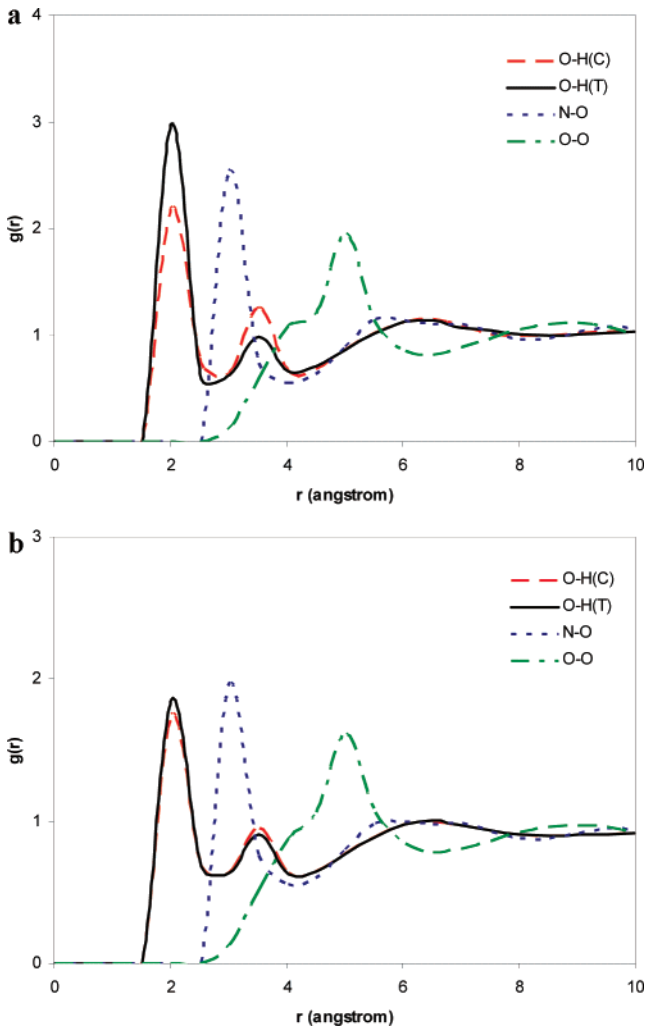

Figure 2. Computed O−H(C), O−H(T), N−O, and O−O radial distribution functions for liquid acetamide at (a) 373 K and (b) 494 K.

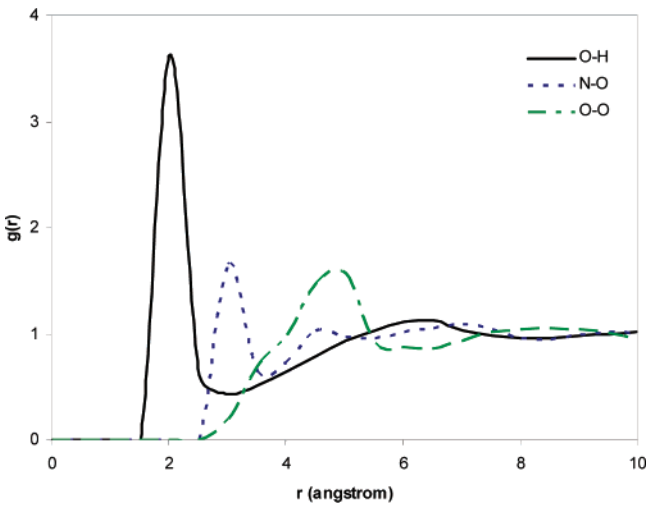

Figure 3. O−H, N−O, and O−O radial distribution functions for liquid *N*-methylformamide at 25 °C.

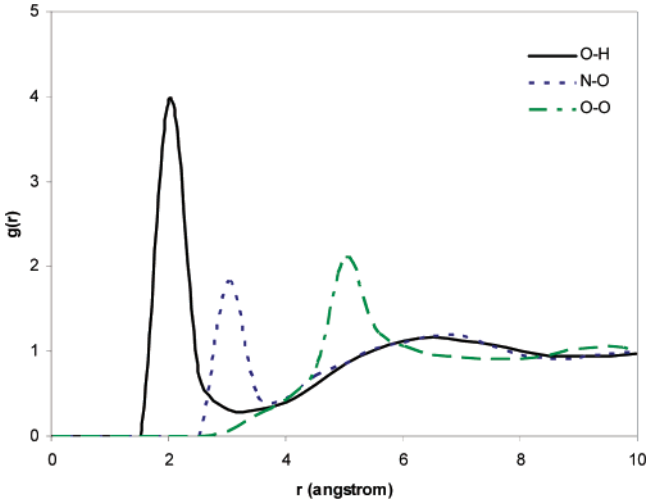

Figure 4. O−H, N−O, and O−O radial distribution functions for liquid *N*-methylacetamide at 100 °C.

0.9 and 1.1 nearest neighbors for these two hydrogen atoms, respectively.[14] Hydrogen bonding interactions are also reflected by the heavy atom distributions, in particular the N−O rdf, which has a strong first peak at 2.93 Å. For comparison, the previous PIPF potential has a peak at 2.8 Å in the N−O distribution.[14] Excellent agreement has been observed with OPLS potential which gives a peak at 2.9 Å. Integration of the first peak to the minimum at 4.02 Å yields 3.41 contacts. This is greater than the finding from previous PIPF and OPLS potentials, which yield a value of 2.5−2.7. Different diffraction studies produced values of 2.9, 3.03, and 3.05 Å,[71−74] reflecting the uncertainty range from experiments. We note that the computed contact number depends strongly on the minimum position in the rdf, which is often not precisely defined due to overlap between the tails from the first and second solvation layers.

The computed rdfs for acetamide are displayed in Figure 2 at two simulation temperatures, corresponding to 373 and 494 K. The first peaks in the N−O distribution function are found at 2.90 and 2.93 Å at 373 and 494 K, respectively, which are slightly shorter than a distance of 3.03 Å from a recent X-ray diffraction experiment of liquid acetamide at 346 K.[75] An important qualitative feature is that the heights of the two O−H peaks decrease noticeably as the temperature increases, suggesting greater thermal fluctuations and less structured interactions. Figure 2a also reveals that the trans hydrogen, H(T), dominates hydrogen bonding interactions due to favorable dipolar orientations, which is also indicated in Figure 1. However, at higher temperature, the contributions from both hydrogens in hydrogen bonding interactions become similar. Integration of the first peaks in O−H(C), O−H(T), and N−O rdfs to the first minima results in 0.8, 0.9, and 2.4 nearest neighbors at 373 K. At higher temperature, the number of the first contacts decreases to 0.7, 0.7, and 2.0.

4.3.2. N-Methylformamide and N-Methylacetamide. The computed rdfs for NMF and NMA are displayed in Figures 3 and 4. Strong hydrogen bonding in these two liquids is clearly indicated by the first striking peaks in the O−H and N−O rdfs. The computed rdf for O−H shows a strong peak at 1.95 Å for both NMF and NMA, in good agreement with the neutron diffraction experiment with fully deuterated NMF which gives the O−H contact at 1.89 Å.[76,77] Integration to the first minima gives 1.0 and 1.1 nearest neighbors in liquid NMA and NMF, respectively. The other peak extensively

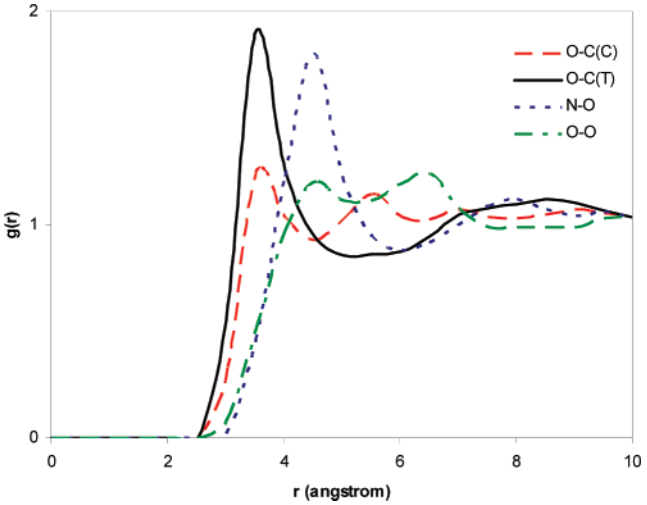

Figure 5. O−C(C), O−C(T), N−O, and O−O radial distribution functions for liquid *N,N*-dimethylformamide at 25 °C. C(C) and C(T) specify the methyl carbon atoms cis and trans to the carbonyl group.

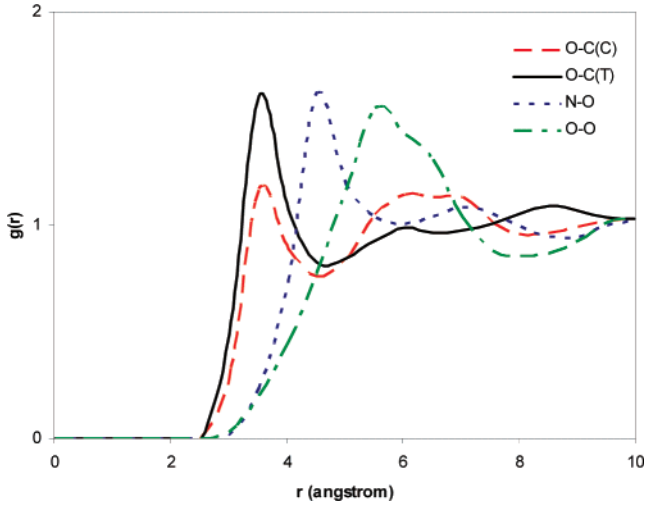

Figure 6. O−C(C), O−C(T), N−O, and O−O radial distribution functions for liquid *N,N*-dimethylacetamide at 25 °C. C(C) and C(T) specify the methyl carbon atoms cis and trans to the carbonyl group.

studied by diffraction experiments is the peak in N−O rdf. The N−O interaction due to hydrogen bonding in liquid NMF and NMA are estimated to be 3.02 Å for NMF in X-ray diffraction[76,77] and 3.03 Å for NMA from both diffraction experiment and DFT calculations.[78] Our calculation gives a value of 2.90 and 2.93 Å in liquid NMF and NMA, respectively. Integration to the first minima yields 1.1 and 1.2 for NMA and NMF, respectively. In contrast, MC simulations from previous study using PIPF-A force field give the first peak at 1.85 and 2.75 Å for O−H and N−O contact, respectively.[14]

We note that the present PIPF potential employing the TID model for polarization yields N−O peaks for the primary and secondary amides in close agreement (2.90−2.95 Å from simulations vs 3.03 Å from diffraction experiments), which may be compared with previous simulations (2.75−2.8 Å) employing a polarizable potential and the Applequist-like polarizabilities.[14] Furthermore, it has often been suggested that it is necessary to have shorter hydrogen-bonding peaks in liquid simulations with effective pair potentials to account for polarization effects by making stronger and shorter hydrogen bonds. For example, the OPLS force field has a distance of 2.9 Å at the first peaks in the N−O rdfs for formamide and NMA.[79] We also notice that the height of the first peak and shape in the N−O rdf for NMA, including a shoulder at about 4.5 Å and a broad peak at about 7 Å, are found to be in good agreement between the present PIPF and OPLS force field.

4.3.3. N,N-Dimethylformamide and N,N-Dimethylacetamide. Despite the fact that there is no hydrogen bond donor in DMF and DMA, the computed rdfs displayed in Figures 5 and 6 show significant local order due to the interaction between methyl groups and carbonyl oxygen in the view of the peaks in O−C(C) and the O−C(T) rdfs centered at 3.50 Å and the N−O rdf at 4.55 Å. This is consistent with the conclusions of Jorgensen and Swenson using the OPLS-UA potential[79] and our PIPF-A model.[14] Interestingly, dipolar interactions favor closer contacts between the trans methyl group and the carbonyl oxygen in both the present and early PIPF potentials. On the other hand, the OPLS-UA potential does not seem to distinguish between the two methyl groups in DMF.[79] In contrast, X-ray diffraction experiments suggest no significant local order in liquid DMF and DMA;[80,81] however, it is difficult to specifically resolve the total diffraction pattern into specific pair interactions without significant hydrogen bonding interactions and isotope replacement.

Table 5. Torsional Terms and Parameters That Have Been Adjusted from the Original CHARMM22 Force Field for use in Connection with the Present PIPF Potential for Amides

dihedral type	K_φ	n	δ
CT3−C−NH1−CT3	1.2	1	0
CT3−CT1−NH1−C	1.6	1	0
HA−CT3−NH1−H	0.11	3	0
O−C−CT3−HA	0.04	3	180

Table 6. Relative Energies (in kcal/mol) and Conformations (in deg) of the Alanine Dipeptide $C7_{eq}$, $C7_{ax}$, and C5 Minima from Ab Initio (LMP2/cc-pVQZ(-g)//MP2/6-31G(p,d)) and Force Field Calculations (ref 49)

	$C7_{eq}$	$C7_{ax}$	C5
QM	0	2.20	1.01
PIPF	0	1.97	1.53
	Conformations (ϕ,ψ)		
QM	−83, 78	74, −64	−158, 162
PIPF	−79, 77	69, −73	−152, 156

4.4. Internal Parameters. The internal bonded parameters are reoptimized for amides functional groups making use of NMA and alanine "dipeptide" as the model compounds. We began with the original CHARMM22 force field for all bonding terms, and it was found that all parameters associated with bonds and angles and with the improper dihedral angle terms can be kept without alteration. The only

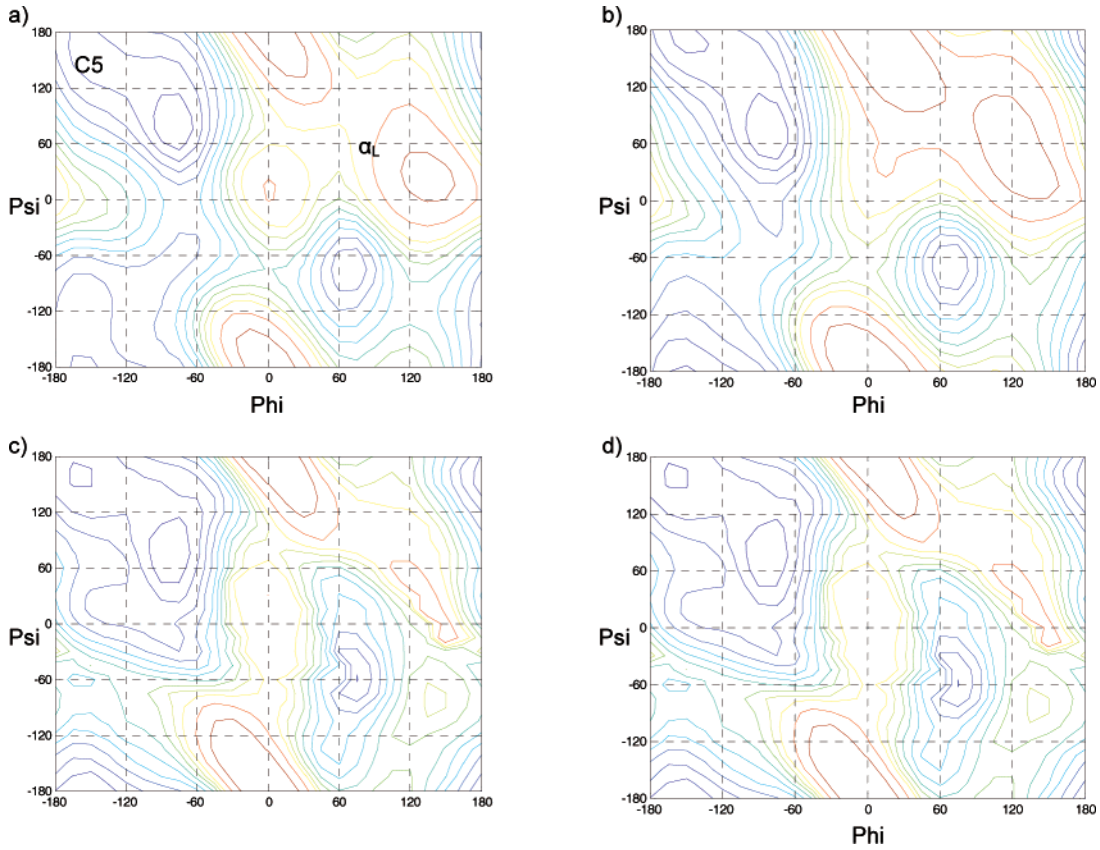

Figure 7. Adiabatic alanine dipeptide potential energy surface calculated from (a) PIPF, (b) CHARMM22, (c) PIPF with CMAP, and (d) QM. Contour represents 1−10 kcal/mol with 1 kcal/mol interval, 12 kcal/mol, and 15 kcal/mol.

parameters that were further modified are some torsional terms, which are listed in Table 5. These values are optimized to reproduce ab initio conformation energies of NMA and the potential energy surface (Ramachandran map) of alanine dipeptide.

With these minor readjustments of the CHARMM22 parameters, we found that it is possible to obtain the relative conformational energies for NMA and the alanine dipeptide using the present polarizable nonbonded interaction terms. In particular, we found that cis conformer of NMA is 2.44 kcal/mol higher in energy than the trans configuration, and the rotation barrier about the peptide bond is 21.1 kcal/mol. For comparison, MP2/cc-pVTZ//MP2/6-31G(d) calculations yield values of 2.39 and 20.5 kcal/mol, respectively.[27] NMR studies revealed a rotational barrier of 19.8 ± 1.8 kcal/mol.[82] The relative conformational energies for the alanine dipeptide are given in Table 6, which are compared with QM calculations at LMP2/cc-pVQZ(-g)//MP2/6-31G(d) level. The relative energy of $C7_{ax}$ calculated by the present force field is underestimated by 0.2 kcal/mol, while the energy of C5 is overestimated by 0.5 kcal/mol. The largest deviation was found in the Ψ angle for the $C7_{ax}$ conformer, which is overestimated by nearly 20° at −73° compared to −64° from LMP2/cc-pVQZ(-g)//MP2/6-31+G(d) calculations.

Ramachandran plot (phi−psi map) computed using the present CHARMM-PIPF potential, the original CHARMM22 force field, and the ab initio MP2/TZVP//6-31G(d,p) are shown in Figure 7, along with a fully corrected energy contour by the CMAP (see below) procedure. In comparison with the MP2 results, the CHARMM22 force field shows a steep surface at the C5 region, and the energy in the α_L region is overestimated. The PIPF-CHARMM force field yields somewhat improved features in these two regions. As noted elsewhere,[49] artifacts exist to overly sample the π-helical populations using empirical potentials, whereas π-helices are rarely observed experimentally. This problem was traced to subtle deviations between the empirical and ab initio Ramachandran maps. MacKerell et al.[49] made a bold proposal by introducing a spline correction map (CMAP) to reproduce almost exactly the MP2 results. Now, the CMAP is a standard option in the CHARMM22 force field, which significantly improved conformational sampling of low population structures. A CMAP has also been constructed for the present CHARMM-PIPF potential, which gives a mean deviation from the MP2 results by merely 0.0002 kcal/mol.

As in the standard CHARMM force field, we have two options that the users may choose from, with and without the inclusion of the CMAP for the PIPF-CHARMM potential. The use of CMAP slightly increases computational time. If this is not a major concern, it is recommended to include the CMAP procedure because it significantly reduces the tendency to form a π-helix.

The transferability of the bond and angle parameters from the CHARMM22 force field is further tested by vibrational spectral analysis of NMA and three conformers of the alanine dipeptide. Calculated frequencies and key characteristic components for each mode have been determined for each molecule; these results are given as Supporting Information in Tables S1−S4. Comparison with experimental and ab

initio results at the LMP2/cc-pVQZ(-g)//MP2/6-31G(d) level of theory suggest that only small differences exist for lower frequency modes between the polarizable force field and the CHARMM22 force field, and the agreement with ab initio force field analyses is are also of similar quality both in computed vibrational frequencies and contributing vibrational motions.

5. Conclusions

A polarizable intermolecular potential function (PIPF) employing the Thole interacting dipole (TID) polarization model has been developed for liquid alkanes and amides. In connection with the internal force field terms of the CHARMM22 force field, with minor modifications of several torsional terms only, the present PIPF-CHARMM potential provides an adequate description of structural and thermodynamic properties for liquid alkanes and for liquid amides. The computed heats of vaporization and liquid density are within 1.4% of experimental values. Although polarization effects are negligible in liquid alkanes, they make major contributions to the potential energy of liquid amides. The average molecular dipole moments are enhanced by 1.5−1.8 D for primary and secondary amides, from gas-phase values of about 3.3−3.7 D to condensed-phase values of 5−5.4 D. This represents as large as a 50% increase from induction polarizations and is reflected by the computed polarization contributions, ranging from 6 to 24% of total potential energies. The average induced dipoles are nearly twice as large as a previous set of polarizable potentials, making use of Applequist-like atomic polarizabilities without intramolecular interactions, but they are in closer agreement with combined QM/MM simulations in which one molecule of amide was treated quantum-mechanically in a liquid of the same amides represented classically.[14] The ability of the PIPF-CHARMM force field to treat protein backbone structures is tested by examining the potential energy surface of the amide bond rotation in *N*-methylacetamide and the Ramachandran surface for alanine dipeptide. The agreement with ab initio MP2 results and with the original CHARMM22 force field is encouraging, suggesting the PIPF-CHARMM potential can be used as a starting point to construct a complete polarizable force field for proteins.

Acknowledgment. This work was partially supported by the National Institutes of Health.

Supporting Information Available: Four tables containing results from vibrational force field analyses using the present PIPF-CHARMM potential, the CHARMM22 force field, and ab initio LMP2/cc-pVQZ(-g)//MP2/6-31G-(p,d) method plus a full listing of the PIPF-CHARMM force field parameters for alkanes and amides. This material is available free of charge via the Internet at http://pubs.acs.org.

References

(1) MacKerell, A. D., Jr. Empirical Force Fields for Biological Macromolecules: Overview and Issues. *J. Computat. Chem.* **2004**, *25*, 1584–1604.

(2) Allen, M. P.; Tildesley, D. J. *Computer Simulations of Liquids*; Oxford University Press: London, 1987.

(3) Stillinger, F. H.; Weber, T. A.; David, C. W. *J. Chem. Phys.* **1982**, *76*, 3131.

(4) Van Belle, D.; Couplet, I.; Prevost, M.; Wodak, S. J. *J. Mol. Biol.* **1987**, *198*, 721.

(5) Niesar, U.; Corongiu, G.; Clementi, E.; Kneller, G. R.; Bhattacharya, D. K. *J. Phys. Chem.* **1990**, *94*, 7949.

(6) Sprik, M.; Klein, M. L.; Watanabe, K. *J. Phys. Chem.* **1990**, *94*, 6483.

(7) Wallqvist, A.; Berne, B. J. *J. Phys. Chem.* **1993**, *97*, 13841.

(8) Rick, S.; Stuart, S;, Berne, B. *J. Chem. Phys.* **1994**, *101*, 6141.

(9) Bernardo, D. N.; Ding, Y.; Krogh-Jespersen, K.; Levy, R. M. *J. Comput. Chem.* **1995**, *16*, 1141.

(10) Ding, Y.; Bernardo, D. N.; Krogh-Jespersen, K.; Levy, R. M. *J. Phys. Chem.* **1995**, *99*, 11575.

(11) Caldwell, J. W.; Kollman, P. A. *J. Phys. Chem.* **1995**, *99*, 6208.

(12) Cieplak, P.; Caldwell, J.; Kollman, P. *J. Comput. Chem.* **2001**, *22*, 1048.

(13) Gao, J.; Habibollazadeh, D.; Shao, L. *J. Phys. Chem.* **1995**, *99*, 16460.

(14) Gao, J.; Pavelites, J. J.; Habibollazadeh, D. *J. Phys. Chem.* **1996**, *100*, 2689.

(15) Stern, H. A.; Kaminski, G. A.; Banks, J. L.; Zhou, R.; Berne, B. J.; Friesner, R. A. *J. Phys. Chem. B* **1999**, *103*, 4730.

(16) Maple, J. R.; Cao, Y.; Damm, W.; Halgren, T. A.; Kaminski, G. A.; Zhang, L. Y.; Friesner, R. A. *J. Chem. Theory Comput.* **2005**, *1*, 694.

(17) Ren, P.; Ponder, J. W. *J. Comput. Chem.* **2002**, *23*, 1497.

(18) Ren, P.; Ponder, J. W. *J. Phys. Chem. B* **2003**, *107*, 5933.

(19) Rasmussen, T. D.; Ren, P.; Ponder, J. W.; Jensen, F. *Int. J. Quantum Chem.* **2007**, *107*, 1390.

(20) Lamoureux, G.; Roux, B. *J. Chem. Phys.* **2003**, *119*, 3025.

(21) Vorobyov, I. V.; Anisimov, V. M.; MacKerell, A. D., Jr. *J. Phys. Chem. B* **2005**, *109*, 18988.

(22) Patel, S.; Brooks, C. L. *J. Comput. Chem.* **2004**, *25*, 1.

(23) Patel, S.; Mackerell, A. D., Jr.; Brooks, C. L., III *J. Comput. Chem.* **2004**, *25*, 1504.

(24) Patel, S.; Brooks, C. L., III *J. Chem. Phys.* **2005**, *123*, 164502.

(25) Ponder, J. W.; Case, D. A. *Adv. Prot. Chem.* **2003**, *66*, 27.

(26) Halgren, T. A.; Damm, W. *Curr. Opin. Struct. Biol.* **2001**, *11*, 236.

(27) MacKerell, A. D., Jr.; Bashford, D.; Bellott, M.; Dunbrack, R. L., Jr.; Evanseck, J. D.; Field, S.; Fischer, M. J.; Gao, J.; Guo, H.; Ha, S.; Joseph-McCarthy, D.; Kuchnir, L.; Kuczera, K.; Lau, F. T. K.; Mattos, C.; Michnick, S.; Ngo, T.; Nguyen, D. T.; Prodhom, B.; Reiher, W. E., III; Roux, B.; Schlenkrich, M.; Smith, J. C.; Stote, R.; Straub, J.; Watanabe, M.; Wiorkiewicz-Kuczera, J.; Yin, D.; Karplus, M. *J. Phys. Chem. B* **1998**, *102*, 3586.

(28) Jorgensen, W. L.; Tirado-Rives, J. *J. Am. Chem. Soc.* **1988**, *110*, 1657.

(29) Gao, J. *J. Phys. Chem. B* **1997**, *101*, 657.

(30) Gao, J. *J. Chem. Phys.* **1998**, *109*, 2346.

(31) (a) Car, R.; Parrinello, M. *Phys. Rev. Lett.* **1985**, *55*, 2471. (b) Chen, B.; Ivanov, I.; Klein, M. C.; Parrinello, M. *Phys. Rev. Lett.* **2003**, *91*, 215503.

(32) (a) Grossman, J. C.; Schwegler, E.; Draeger, E. W.; Gygi, F.; Galli, G. *J. Chem. Phys.* **2004**, *120*, 300. (b) Kuo, I.-F. W.; Mundy, C. J. *Science* **2004**, *303*, 658.

(33) (a) Morgantini, P.-Y.; Kollman, P. A. *J. Am. Chem. Soc.* **1995**, *117*, 6057. (b) Menge, E. C.; Caldwell, J. W.; Kollman, P. A. *J. Phys. Chem.* **1996**, *100*, 2367. (c) Ding, Y.; Bernardo, D. N.; Krogh-Jespersen, K.; Levy, R. M. *J. Phys. Chem.* **1995**, *99*, 11575. (d) Marten, B.; Kim, K.; Cortis, C.; Friesner, R. A.; Murphy, R. B.; Ringnalda, M. N.; Sitkoff, D.; Honig, B. *J. Phys. Chem.* **1996**, *100*, 11775. (e) Rizzo, R. C.; Jorgensen, W. L. *J. Am. Chem. Soc.* **1999**, *121*, 4827.

(34) (a) Stuart, S. J.; Berne, B. J. *J. Phys. Chem.* **1996**, *100*, 11934. (b) Stuart, S. J.; Berne, B. J. *J. Phys. Chem. A* **1999**, *103*, 10300.

(35) Dang, L. X.; Chang, T.-M. *J. Chem. Phys.* **1997**, *106*, 8149.

(36) Rick, S. W.; Stuart, S. J. *Rev. Comput. Chem.* **2002**, *18*, 89.

(37) Sprik, M.; Klein, M. L. *J. Chem. Phys.* **1998**, *89*, 7556.

(38) Nadig, G.; Van, Zant, L. C.; Dixon, S. L.; Merz, K. M., Jr. *J. Am. Chem. Soc.* **1998**, *120*, 5593.

(39) Sanderson, R. T. *Science* **1951**, *114*, 670.

(40) Parr, R. G.; Yang, W. *Density-functional Theory of Atoms and Molecules*; Oxford University Press: Oxford, 1989.

(41) Mortier, W. J.; Ghosh, S. K.; Shankar, S. *J. Am. Chem. Soc.* **1986**, *108*, 4315.

(42) Rappé, A. K.; Goddard, W. A. *J. Phys. Chem.* **1991**, *95*, 3358.

(43) York, D. M.; Yang, W. *J. Chem. Phys.* **1996**, *104*, 159.

(44) Banks, J. L.; Kaminski, G. A.; Zhou, R.; Mainz, D. T.; Berne, B. J.; Friesner, R. A. *J. Chem. Phys.* **1999**, *110*, 741.

(45) Jorgensen, W. L.; Maxwell, D. S.; Tirado-Rives, J. *J. Am. Chem. Soc.* **1996**, *118*, 11225.

(46) Thole. B. T. *Chem. Phys.* **1981**, *59*, 341.

(47) van Duijnen, P. T.; Swart, M. *J. Phys. Chem. A* **1998**, *102*, 2399.

(48) Van Belle, D.; Froeyen, M.; Lippens, G.; Wodak, S. *Mol. Phys.* **1992**, *77*, 239.

(49) MacKerell, A. D., Jr.; Feig, M.; Brooks, C. L., III. *J. Comput. Chem.* **2004**, *25*, 1400.

(50) Hoover, W. G. *Phys. Rev. A* **1985**, *31*, 1695.

(51) Feller, S. E.; Zhang Y.; Pastor, R. W.; Brooks, B. R. *J. Chem. Phys.* **1995**, *103*, 4613.

(52) Martyna, G. J.; Tuckerman, M. E.; Tobias, D. J.; Klein, M. L. *Mol. Phys.* **1996**, *87*, 1117.

(53) (a) Horn, H. W.; Swope, W. C.; Pitera, J. W.; Madura, J. D.; Dick, T. J.; Hura, G. L.; Head-Gordon, T. *J. Chem. Phys.* **2004**, *120*, 9665. (b) Horn, H. W.; Swope, W. C.; Pitera, J. W. *J. Chem. Phys.* **2005**, *123*, 194504/1. (c) Steinbach, P. J.; Brooks, B. R. *J. Comput. Chem.* **1994**, *15*, 667.

(54) Ryckaert, J. P.; Ciccotti, G.; Berendsen, H. J. C. *J. Comput. Phys.* **1977**, *23*, 327.

(55) Lide, D. R. *CRC Handbook of Chemistry and Physics*; CRC Press: U.S.A., 2006.

(56) Yaws, C. L. *Chemical Properties Handbook*; McGraw-Hill, 1999.

(57) Riddick, J. A.; Bunger, W. B. *Organic Solvents*, 3rd ed.; Wiley-Interscience: New York, 1970.

(58) Applequist, J.; Carl. J. R.; Fung, K. *J. Am. Chem. Soc.* **1972**, *94*, 2952.

(59) Jorgensen, W. L; Madura, J. D.; Swenson, C. J. *J. Am. Chem. Soc.* **1984**, *106*, 6638.

(60) Daubert, T. E.; Bartakovits, R. *Ind. Eng. Chem. Res.* **1989**, *28*, 641.

(61) Reid, R. C.; Praunitz, J. M; Poling, B. E. *The Properties of Gases and Liquids*, 4th ed.; McGraw-Hill: New York, 1987; pp 42, 97, 136−143, 209.

(62) Lemire, R. J.; Sears, P. G. *Top. Curr. Chem.* **1978**, *74*, 45.

(63) Covington, A. K.; Dickinson, *T. Physical Chemistry of Organic Solvent Systems*; Plenum: London, 1973.

(64) Gopal, R.; Rigzi, ***S.*** A. *J. Ind. Chem. Soc.* **1966**, *43*, 179.

(65) Geller, B. Zegers, H. C.; Somsen, *G. J. Chem. Thermodyn.* **1984**, *16*, 225.

(66) Somsen, G.; Coops, J. *Rec. Trau. Chim.* **1965**, *84*, 985.

(67) Radzicka, A.; Wolfenden, R. *Biochemistry* **1988**, *27*, 1664.

(68) Drakenberg, T.; Dahlqvist, K.-I.; Forsen, S. *J. Chem. Phys.* **1972**, *76*, 2178.

(69) Greiner-Schmid, A.; Wappmann, S.; Has, M.; Lüdemann, H.-D. *Chem. Phys.* **1991**, *94*, 5643.

(70) Chen, L.; Gross, T.; Lüdemann, H.-D. *Z. Phys. Chem. (Muenchen)* **2000**, *214*, 239.

(71) Kalman, E.; Serke, I.; Palinkas, G.; Zeidler, M. D.; Wiesmann, F. J.; Bertagnolli, H.; Chieuz, P. *Z. Naturforsch., A: Phys. Sci*. **1983**, *38A*, 231.

(72) DeSando, R. J.; Brown, G. H. *J. Phys. Chem.* **1968**, *72*, 1088.

(73) Ohtaki, H.; Funaki, A.; Rode, B. M.; Reibnegger, G. J. *Bull. Chem. Soc. Jpn.* **1983**, *56*, 2116.

(74) Ohtaki, H.; Katayama, N.; Ozutsumi, K.; Radnai, T. *J. Mol. Liq.* **2000**, *88*, 109.

(75) Nasr, S.; Mounir, Ghédira, M.; Cortès, R. *J. Chem. Phys.* **1999**, *110*, 10487.

(76) Hammami, F.; Nasr, S.; Bellissent-Funel, M.; Oumezzine, M. *J. Phys. Chem. B* **2005**, *109*, 16169.

(77) Hammami, F.; Nasr, S.; Oumezzine, M.; Cortès, R. *Biomol. Eng.* **2002**, *19*, 201.

(78) Trabelsi, S.; Bahri, M.; Nasr, S. *J. Chem. Phys.* **2005**, *122*, 024502.

(79) Jorgensen, W. L.; Swenson, C. J. *J. Am. Chem. Soc.* **1985**, *107*, 569.

(80) Borrmann, H.; Persson, I.; Sandström, M.; Stålhandske, C. M. V. *J. Chem. Soc., Perkin Trans.* **2000**, *2*, 393.

(81) Takamuku, T.; Matsuo, D.; Tabata, M.; Yamaguchi, T.; Nishi, N. *J. Phys. Chem. B* **2003**, *107*, 6070.

(82) Drakenberg, T.; Forsén, S. *Chem. Commun.* **1971**, *21*, 1404.

CT700146X